# Super-resolution within a one-dimensional phononic crystal of resonators using time reversal in an equivalent circuit model

Adam D. Kingsley, Brian E. Anderson and T. J. Ulrich

# Super-resolution within a one-dimensional phononic crystal of resonators using time reversal in an equivalent circuit model

Adam D. Kingsley,[1] Brian E. Anderson,[1,a)] (ID) and T. J. Ulrich[2] (ID)

[1]*Acoustics Research Group, Department of Physics and Astronomy, Brigham Young University, Provo, Utah 84602, USA*

[2]*Los Alamos National Laboratory, Los Alamos, New Mexico 87545, USA*

**ABSTRACT:**

An equivalent circuit model has been developed to model a one-dimensional waveguide with many side-branch Helmholtz resonators. This waveguide constitutes a phononic crystal that has been shown to have decreased phase speed below the resonance frequency of an individual resonator. This decreased phase speed can be exploited to achieve super-resolution using broadband time reversal focusing techniques. It is shown that the equivalent circuit model is capable of quantifying this change in phase speed of the crystal and also the small-scale wave-resonator interactions within the crystal. The equivalent circuit model enables the parameterization of the physical variables and the optimization of the focusing bandwidth by balancing the combination of increasing resolution and decreasing amplitude near the resonance frequency. It is shown that the quality factor—in this case, the quality factor determined by the geometric shape of each resonator—controls the range of frequencies that are strongly affected by the Helmholtz resonators. © *2022 Acoustical Society of America.* https://doi.org/10.1121/10.0013832

## I. INTRODUCTION

Time reversal (TR) is a signal processing method to obtain a focus of waves.[1–3] Originally called matched signal processing,[4,5] it combines an exploration step (forward step), where the impulse response is obtained, with a focusing step (backward step), which uses the time-reversed impulse response to generate a constructive interference of waves. First used in underwater acoustics, TR has found application in several fields, including seismology,[6] lithotripsy,[7] and nondestructive evaluation.[3]

TR has been used to localize acoustic sources. Applications include locating finger taps to use a solid media as a touch interface,[8] localizing the source of a gunshot in an urban environment,[9] and localizing and characterizing the great Sumatra earthquake.[10] These methods of localization require a backward step that is performed by modeling the environment, including scatterers, and numerically back propagating the impulse response signals from the receivers to find a point of maximum convergence. TR localization and imaging is well known to be limited by the diffraction limit, though if the finite size of imaged sources exceeds a half wavelength, then the true spatial extent is clouded by interference in focused waves.[11]

When focusing waves using TR, both direct and scattered waves simultaneously converge to a point in space creating a constructive focus that is diffraction-limited. Focusing to a spatial extent smaller than the diffraction limit is termed super-resolution. The diffraction limit has multiple useful definitions but typically constrains the spatial extent of the converging of waves to be no smaller than a half

wavelength, $\lambda/2$.[12] The primary assumption of the diffraction limit given is that the focus must be in the far field of the source. Several examples exist where super-resolution was achieved in a modified system, several of which used TR. One example is of microwaves focusing among resonators.[13] In this work, the authors placed small antennae receivers among many resonating antennae. Similar work was also done with focusing acoustic waves among soda can resonators,[14] though later it was shown that TR was not necessary due to the regular arrangement.[15] Super-resolution has also been achieved experimentally by using absorbers[16] surrounding the focus as well as numerically[17] by simulating a similar region of absorption near the focus. Obtaining super-resolution with TR has also been demonstrated with near field amplification[18] and by using an active acoustic sink[19] as well as a passive acoustic sink.[20] Each of these examples was done with objects located within or information obtained within the near field.[21]

As described by Maznev *et al.*,[12] the diffraction limit cannot be broken. They assert that sub-diffraction-limited focusing is only possible when violating an assumption of the diffraction limit. A simple physical explanation is that the waves will conform to boundary conditions with perhaps higher spatial frequency than the wave contained elsewhere. Applying this additional restriction would mean that the diffraction limit requires that the focus not only must be in the far field of the source but also must be in the far field of any subwavelength objects. Focusing in a phononic crystal clearly violates this restriction, so although the diffraction limit is not being broken, according to this definition, the properties of the crystal allow for super-resolution focusing compared to waves outside the crystal.

a)Electronic mail: bea@byu.edu

The spatial extent of a TR focus in a one-dimensional (1-D) system is limited by principles like those in diffraction-limited systems. Although in the 1-D case, there is no aperture for diffraction to occur, the interference of direct and scattered waves creates a focal peak limited by the smallest wavelength. Because the measurement axis is the same as the propagation direction, there is no increase in measured wavelength due to oblique angles of approach.

Previous work in TR has shown that focusing near resonators or absorbers can produce a spatial focus much smaller than a wavelength. In this paper, a 1-D duct with periodic side-branch resonators is modeled that constitutes a phononic crystal.[22] This model has been studied in the context of transmission spectra,[23] band structure,[24] and the influence of detuned resonators.[25] However, previous studies[26,27] use an effective medium approach, and the resonators' effect is spread over the length of the duct. To predict the wave-focusing ability that TR offers in this system, it is essential to know the influence of resonator geometric properties as well as focus position relative to resonator position.[15] In essence, the equivalent circuit model allows characterization of the wave field within the crystal.

The purpose of this paper is to present an equivalent circuit model of focusing waves in a duct with many resonators, using TR. Typically, the TR process involves measuring an impulse response, $h_{A,B}$, between two points (A and B), reversing that impulse response (flipping it in time), and playing the reversed impulse response from one of the two points, which can result in focused energy at the other point.[1–3] Tanter *et al.* mention that TR focusing is equivalent to an autocorrelation of an impulse response.[28] More specifically, simulating TR in the time domain consists of obtaining $h_{A,B}$ and then performing an auto-correlation of $h_{A,B}$, thereby obtaining the temporal response ("focal signal") at point B due to broadcasting the time-reversed impulse response, $h_{A,B}(-t)$, from point A. Mathematically, this is calculated as

$$r_B(t) = h_{A,B}(-t) * h_{A,B}(t), \tag{1}$$

where $r_B$ is the response of the signal at point B. When calculating the response at other locations (such as point C) due to the broadcast of $h_{A,B}(-t)$, the response becomes

$$r_C(t) = h_{A,B}(-t) * h_{A,C}, \tag{2}$$

where $r_C$ is the response at point C while focusing occurs at point B. In the frequency domain, an auto-correlation is an auto-spectrum, and the cross correlation is a cross-spectrum. Thus, the temporal relations become spectral relations through a simple Fourier transformation,

$$h_{A,B}(t) * h_{A,B}(-t) \rightarrow H_{A,B}(\omega)H_{A,B}^*(\omega) \tag{3a}$$

and

$$h_{A,C}(t) * h_{A,B}(-t) \rightarrow H_{A,C}(\omega)H_{A,B}^*(\omega). \tag{3b}$$

Note that $*$ denotes a convolution, whereas * denotes a complex conjugation. A parametric study of the quality factor of the resonators and focusing position on the spatial extent and amplitude of waves in the duct is also presented. It is shown that the focusing bandwidth and resolution can be improved by using resonators with low absorption and a low quality factor. The model presented here enables a quick study of many other physical properties of interest. Note that continuous waves are employed here, which can be focused with TR even with single frequencies.[29]

Equivalent circuit, or lumped element, models have been used in acoustics[30] to study 1-D systems and the interaction of waves with side branches, changing cross section, and arbitrary impedances.[31–36] This model can only explore the plane wave propagation of waves in the duct, and consequently, side branches occur at discrete points along the duct rather than over an area. However, this simplified approach allows for faster numerical studies of physical parameters over a range of frequencies.

## II. EQUIVALENT CIRCUIT MODEL

The equivalent circuit model utilizes electrical elements that represent lumped acoustic elements but also includes complex, frequency-dependent impedance elements to account for the phase changes of the wave as it propagates some distance. To model an infinite domain outside the region of resonators, anechoic terminations are added to both ends of the duct as resistors. An anechoic termination matches the characteristic acoustic impedance of the duct (with a resistance value of $\rho_0 c/S$), where $\rho_0$ is the density of air, $c$ is the speed of sound, and $S$ is the cross-sectional area of the duct. This impedance element simulates a semi-infinite duct. This element also eliminates the standing waves that would be created in a duct of finite length, which we want to avoid since the standing waves can overshadow the effects we are trying to study.

Sources can be added as side branches in the duct. The equivalent circuit represents the source by placing it in parallel with the anechoic termination. This implies that some of the energy radiated by the source propagates toward the network of resonators, and some directly propagates toward the anechoic termination. Loudspeakers can be modeled as constant current sources because their internal impedance is much higher than $\rho_0 c/S$. The source strength is chosen to be unity in the appropriate units as the resulting transfer function is ultimately the desired result of the model, and it does not depend on source strength (i.e., linear acoustic propagation is assumed).

Propagation through a duct segment of constant cross section is accomplished by use of the acoustic "T-network."[37] Three reactive, frequency-dependent elements placed in a T-shaped configuration model the proper evolution of the phase as the wave propagates through the circuit (see Fig. 1). The two elements on the horizontal branch of the T are each of value $(j\rho_0 c/S)\tan(kL/2)$, while the element on the vertical branch of the T has a value $-(j\rho_0 c/S)\csc(kL)$.
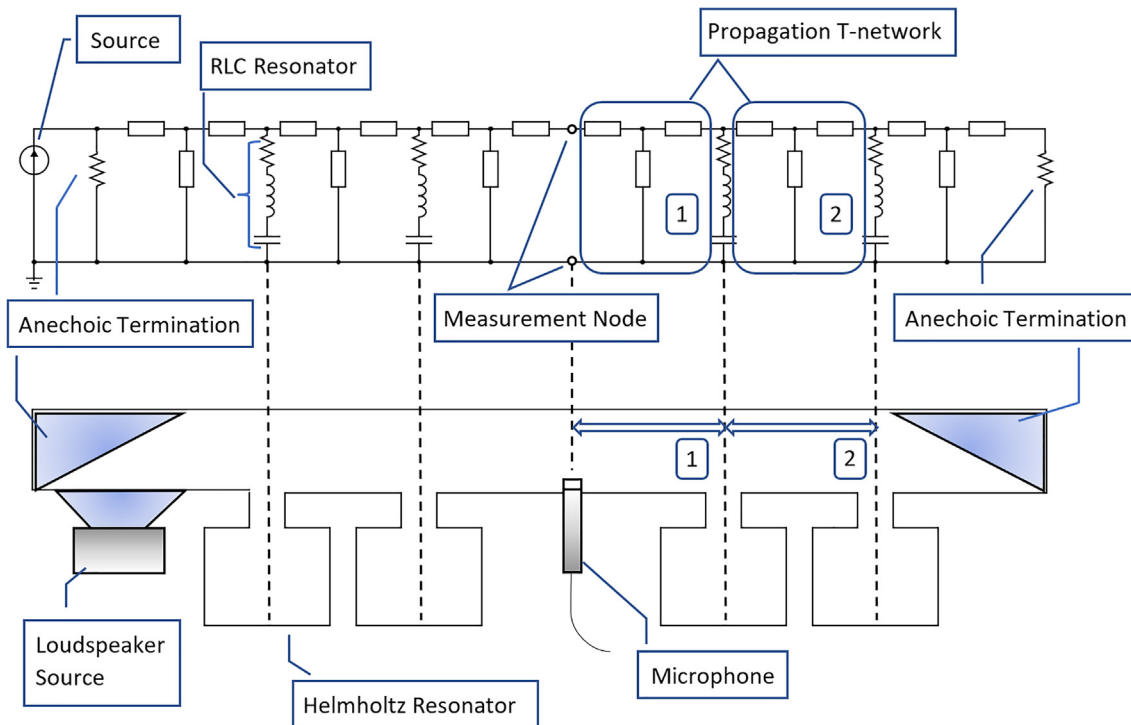
FIG. 1. (Color online) An equivalent circuit model of a waveguide with four side-branch resonators. The equivalent circuit (top) is shown with the corresponding acoustic system (bottom). Dashed lines represent the direct analog between domains. Solid (blue) triangles represent anechoic wedges in the acoustic domain and are modeled as purely resistive, impedance matched elements in the electrical domain. The loudspeaker source is modeled as a current source in the electrical domain. Two of the six "T-networks" for modeling propagation in the electrical domain (labeled [1] and [2]) match the portions of the waveguide that they represent.

Each T-network can span an arbitrary distance with respect to a wavelength of a constant cross section portion of the waveguide just by changing the single length, $L$, parameter (and by modeling the appropriate cross-sectional area). In this model, there is a T-network between the source and the first resonator and then a T-network between each resonator.

An acoustic resonator can be modeled using an equivalent electrical resonating circuit consisting of the series combination of a resistor, inductor, and capacitor, forming an "RLC circuit." The inductive element represents the mass-like inertia of the air in the neck that undergoes a lumped acceleration without compression. This acoustic mass has an equivalent inductance of $M_A = \rho_0 l/S$, where $l$ is the length of the neck (including end corrections) and $S$ is the cross-sectional area of the neck. The volume of the resonator below the neck can be considered a lumped compliance that undergoes compression but no acceleration. The volume is then represented as an equivalent capacitor with a capacitance of $C_A = V/(\rho_0 c^2)$, where $V$ represents the volume of the resonator below the neck. Without any absorptive material in the resonator, the losses are due to thermoviscous effects[38] and can be represented by a resistor with an acoustic impedance value of $R_A = 2mc\alpha_w$, where $m$ is the total acoustic mass of the neck and $\alpha_w$ is the absorption coefficient for wall losses.[39] For the dimensions of the system, the value of the acoustic resistance changes by only $\sim$7% across the frequency band of interest; thus, we obtained a frequency-averaged value for these losses and used this

single number value for $R_A$. The RLC circuit is naturally resonant in the same way the Helmholtz resonator has a single lumped-element resonance. The study presented in this paper uses Helmholtz resonators that always have a resonance frequency of 700 Hz. This frequency was arbitrarily chosen. We expect similar findings to occur for resonators having different frequencies of resonance.

In the assembled circuit, the only circuit nodes exist within the T-network (non-physical) and at the junctions with resonators and sources (see Fig. 1). For arbitrary spacing of measurement points at locations along the waveguide/duct between resonators, additional nodes must be introduced. Measurements of the wave field at locations along the waveguide can be done in the circuit through the introduction of a circuit node represented at the physical location of interest for a measurement. This is accomplished by splitting the T-network into a pair of T-networks that span the same physical distance as the original network. This produces a node between the networks at the measurement position. Calculating the electric potential (i.e., voltage) at the measurement point is equivalent to measuring the acoustic pressure at the physical point in space.

Figure 1 shows a simplified waveguide system with only four resonators in the lower half of the figure. The equivalent electrical circuit is shown above. Circuit elements depicted as boxes represent frequency-dependent impedances with values given previously. The RLC circuit

components are represented by classic electrical imped-ance equation forms for the electric analogs of those acoustic elements. The acoustic system shows a micro-phone measuring the pressure at a point in the waveguide where a node has been introduced in the model by splitting the T-network.

Iterating over a list of measurement points, each produces a unique circuit as each measurement point requires the insertion of a node. Using Kirchhoff's voltage law for loop analysis, the circuit can be formed into a system of equations. Each equation consists of the sum of potential drops over the elements in the loop due to the current in the loop as well as the current in the adjacent loops through shared loop elements. In matrix form, this linear system of equations can be represented as $Z\vec{I} = \vec{V}$, where $Z$ is the matrix of impedance values (here representing acoustic impedances), $\vec{I}$ is the vector of unknown current values (here representing acoustic volume velocities), and $\vec{V}$ is the known net potentials (here representing acoustic pressures) for each loop. The resulting potentials in $\vec{V}$ will all be zero except for the loops that contain a source. Because the source is modeled as an ideal flow source and is in parallel with the anechoic termination, a Thevenin equivalent potential source was substituted that places the new potential source in series with the anechoic element.[40] This reduces the circuit by one loop and provides a known net voltage for that single loop. Solving for the unknown currents can then be done with a numeric linear solver. We used MATLAB's built-in linear solver, mldivide. Once the currents are calculated, the voltage at the measurement point can be calculated by finding the potential relative to ground. This is achieved by calculating the potential drop across the elements that lead to ground. To calculate the potential at the measurement node labeled in Fig. 1, the potential drop along the shortest path to ground is calculated. In the case of Fig. 1, that is two of the elements of propagation T-network [1], just downstream of the node. First the potential across the vertical element is calculated using the currents from the loops on both sides of that element, and then the potential across the left horizontal element is calculated using just the current in that loop. Summing the potential from both elements results in the complex acoustic pressure at that measurement point due to a single source. Solving the circuit at each frequency in the bandwidth provides the desired transfer function between the source and that single measurement point.

After obtaining the transfer function at each measurement point, the spatial extent of TR in the frequency domain is performed by choosing a focal location and calculating the cross-spectra of the transfer function of the target location with the transfer function of every measurement position.[41,42] The resulting set of cross-spectra describe the response at each measurement point when producing a focus at the focal location. Repeating the process for a source at each end and summing the results generated by each of the sources provide the spatial extent of the focus when both sources are active.

To conduct a parametric study of physical parameters, a model was chosen that would remain the same between studies except for the specific parameter to be varied. The model used represents a system with a 3 m long waveguide with a cross-sectional diameter of 10 cm. Cross-modes are not expected in this waveguide until frequencies greater than 2 kHz. A velocity source was added at each end of the duct with equal amplitudes. The resonator region consists of 51 side-branch resonators positioned every 2 cm in the central third of the waveguide from 1 to 2 m. The resonators have a resonance frequency that is held at 700 Hz. The spacing between resonators is $0.04\lambda$ (where $\lambda$ is the wavelength of the resonance frequency) or 2 cm in this case. Measurements are made throughout the duct with a spacing of $0.0025\lambda$ or ~1.2 mm by changing the length variable in the T-network circuit elements. A focus position was chosen to be equally distant between two resonators at 1.51 m (nearly equidistant between the sources). The bandwidth studied was 550–710 Hz.

Figure 2 shows the process of simulating TR focusing for a single source at a single frequency. Figures 2(a) and 2(b) show the magnitude and phase of the transfer function, $H$, between a source and the target focus position with a line marking 625 Hz. Figure 2(c) shows the relative response, $real(H)$, at every position within a duct at this same frequency of 625 Hz. Performing the cross-spectrum between the single value of $H$ at 625 Hz and the response at all positions returns the response everywhere when focusing at this one frequency to this one position. Because Fig. 2 shows the normalized response, this is equivalent to a phase shift that produces a large response at the target focus position. This phase-shifted response is shown in Fig. 2(d). A movie showing the response as a function of phase shift is shown in Mm. 1. This process can be conducted at every frequency,
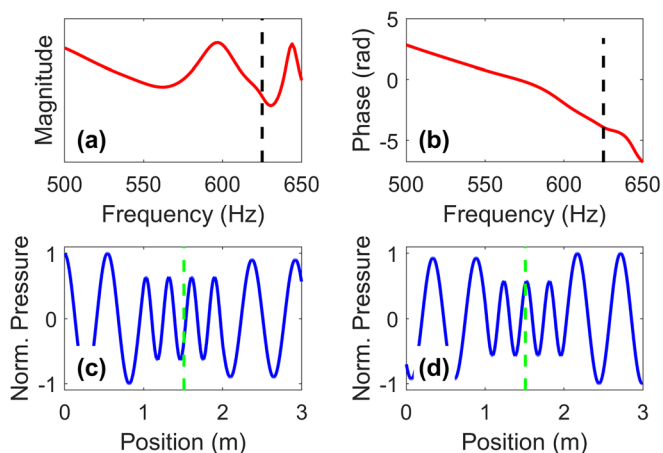


FIG. 2. (Color online) The process of simulating TR in the frequency domain. The magnitude and phase of the frequency response at a target focal location are shown in (a) and (b), with 625 Hz marked with a black, dashed line. The relative response (the real part of the response) throughout the duct is shown in (c). The conjugate of the response at the focal position is then multiplied by the complex response at every position to produce a focus at the target focal location (d).

1266   J. Acoust. Soc. Am. **152** (3), September 2022

Kingsley *et al.*

and the results are summed to produce the response across the whole bandwidth.

Mm. 1. Movie illustrating the phase-shifting of a single frequency to make the source emission produce a positive peak at the focal location. This is a file of type "mp4" (0.8 MB).

In summary, each simulation includes the following steps:

(1) Create a circuit with impedance values calculated for a single frequency.
(2) Split a T-network into two T-networks to create a node where the response can be measured.
(3) Solve the circuit for the flow in every loop of the circuit.
(4) Calculate the potential at the spatial measurement point relative to ground using Ohm's law and the known flows and impedances.
(5) Repeat steps 2–4 for every spatial measurement point in the duct.
(6) Repeat steps 1–5 for every frequency in the bandwidth of interest.
(7) Calculate the cross-spectra between the frequency response at the target focal location and the frequency response at each spatial measurement point.
(8) Sum the real part of the cross-spectrum at each spatial measurement point.
(9) Repeat steps 1–8 for a second source on the other end of the duct.
(10) Superpose results from both sources.

## III. RESULTS

In one dimension, the diffraction limit can be defined as the full width at half maximum (FWHM) of the highest frequency sine wave in the bandwidth. For a sine wave, the half maximum points occur at $kx = [\pi/6, 5\pi/6]$ or, equivalently, $x = [\lambda/12, 5\lambda/12]$. Thus, the FWHM of the pressure distribution of 1-D waves is $\lambda/3$. Figure 3 shows a representative TR focus within the waveguide composed of the focusing that



FIG. 3. (Color online) Focus over a uniform bandwidth of 600–650 Hz. Individual frequencies are shown [(a), (b), and (c)] as examples with the entire combined bandwidth shown on the right (d).

occurs over a range of frequencies. The focus shows a FWHM of $\sim\lambda_{min}/12$, or a fourfold improvement over focusing that would be obtained without the presence of the resonators. By inspecting individual frequencies in Fig. 2, the shortened wavelength components are visible within the resonator region. In the absence of resonators, the waves propagate with a free-space wavelength. Because the interaction of waves near the resonance frequency of a resonator leads to more reflection of those waves, the pressure amplitude drops within the phononic crystal. However, these strong interactions also result in a higher spatial frequency. TR focusing is defined as being at the location where the amplitude is the largest. In the case of Fig. 3(d), the amplitude is largest at the target focal location. However, the neighboring "sidelobe" peaks have significant amplitudes. The amplitude of the sidelobes is largely influenced by the limited bandwidth employed in the focusing, as would be expected from superposition and Fourier analysis. The use of a wider bandwidth reduces the amplitudes of the sidelobes relative to the focal amplitude. Known TR methods for reducing the amplitude of sidelobes include the idea of iterative TR (Ref. 14) and the inverse filter.[28] These methods typically achieve relative sidelobe amplitude reductions at the expense of a lower focal amplitude. In this paper, no additional methods have been applied, and the results use only the most basic TR process. It is important to note that it is more difficult to achieve lower sidelobe amplitudes in a 1-D medium, with only two sources, and using continuous wave TR.[29,43] The focus amplitude is larger because the spatial extent of the focusing at each frequency constructively interferes at that location due to the TR process.[29] Note that frequencies above the resonance frequency do not spatially oscillate and are heavily attenuated by the resonators, and although those frequencies do not contribute significantly to the focus, they do worse than the diffraction limit, resulting in less significant super-resolution (if they are included in the bandwidth).

The focusing achieved at frequencies near resonance lends itself to an analysis of the effective wavelength of each frequency at the focal location. An effective wavelength, $\lambda_{eff}$, for each frequency component, $f$, of the focusing can be found by measuring the FWHM of the peak closest to the target focal location and setting the FWHM equal to $\lambda_{eff}/3$ (the FWHM of a sine wave in a 1-D system). This $\lambda_{eff}$ can be larger or smaller than the free-space wavelength due to the interactions with the resonators. Using $\lambda_{eff}$ and $f$, the phase speed of the wave can be calculated, $v = f\lambda_{eff}$.

Figure 4 shows the phase speed versus frequency for this example network of resonators. Below resonance, the phase speed is below the speed of sound in the model. In this model, the phase speed is below the speed of sound for all frequencies down to 47 Hz with a phase speed of 257 m/s, which is the lowest frequency that can be measured in the domain. Near resonance, the wave field is oscillating with a spatial frequency that matches the physical spacing of the resonators, though with very small amplitudes. However, immediately after crossing the resonance frequency, the wave ceases to spatially oscillate within the resonator
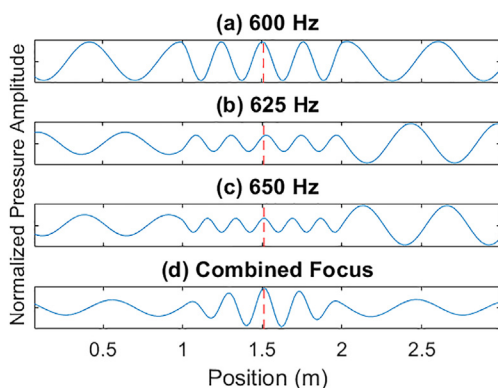
J. Acoust. Soc. Am. 152 (3), September 2022

Kingsley et al. 1267
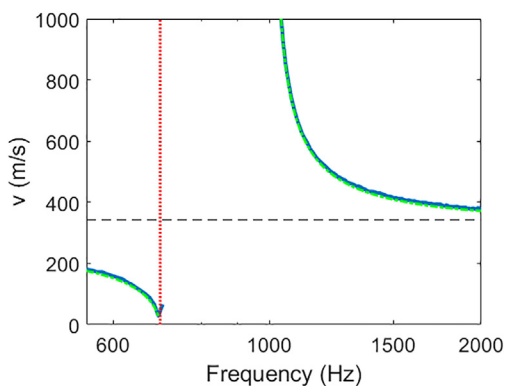
FIG. 4. (Color online) Comparing phase speed between equivalent circuit model and the effective medium approach used by Bradley (Ref. 26) as presented by Sugimoto *et al*. (Ref. 27). Solid blue line, calculated wave speed from the FWHM of the closest peak to the focus. Dotted-dashed green line, from the model presented by Sugimoto *et al*. Dashed black line, bulk wave speed in air. Dotted red line, resonance frequency of an individual resonator. A drop in phase speed is visible below resonance, and above resonance the wave eventually propagates and the phase speed drops to that of the speed of sound in air.

network, and instead the wave exponentially decays across the resonator network. Because the waves do not spatially oscillate in the resonator network, the effective wavelength is greater than the length of the resonator network. At higher frequencies, the acoustic waves do not interact strongly with the resonators, and once again, the signal propagates with effective wavelengths less than the length of resonator network, allowing for the phase speed to be measured. At even higher frequencies, the effective wavelengths eventually return to the normal, plane-propagation wavelengths, and the phase speed converges back to the speed of sound.

To validate the results from the equivalent circuit model, the dispersion relation given by Bradley[26] and later by Sugimoto and Horioka[27] is used to compute a phase speed for the physical system presented here. This phase speed is a large-scale effect of the phononic crystal, and the equivalent circuit model should result in the same phase speed while allowing for finer exploration of the focusing waves. The two systems being modeled are only different in the length of the phononic crystal. The effective medium models use an infinite crystal, but the equivalent circuit model requires a finite length to the phononic crystal. Representation of an infinite domain would require knowing the input impedance to a semi-infinite crystal and using that impedance as the termination on the finite domain. As shown in Fig. 4, the analytical model by Bradley[26] as presented by Sugimoto and Horioka[27] shows excellent agreement with the results from the equivalent circuit model. This agreement lends confidence to the equivalent circuit model approach to explain large- and small-scale interactions with the resonators.

## IV. PARAMETRIC STUDY OF RESONATOR IMPEDANCE

Of the variables used to construct the model, perhaps the most conspicuous is that of the impedance of the

resonators. In previous research utilizing phononic crystals of soda cans, the impact of the resonator shape (and, hence, its impedance or impact on quality factor) on the resolution improvement was not studied. If the frequency bandwidth of study is small compared to the resonance frequency and is close to the resonance frequency, $f_0$, the shape of the impedance curve of the resonators is governed by the mass and compliance of the resonator. The shape of a resonator's impedance curve is often described by the quality factor of the resonator. This acoustic quality factor, $Q$, incorporates three variables, namely, mass, compliance, and resistance,

$$Q = \frac{f_0}{f_u - f_l} = \frac{\omega_0 M_A}{R_A} = \frac{1}{R_A}\sqrt{\frac{M_A}{C_A}}, \tag{4}$$

where $f_u$ and $f_l$ are the half power frequencies above and below $f_0$, respectively, and $\omega_0 = 2\pi f_0 = (M_A C_A)^{-1/2}$ is the angular resonance frequency. Because of the dependence on resistance, the $Q$ is frequently used to study the behavior of a resonator as the damping is changed. For our study, we keep the resistance as well as the resonance frequency the same. However, the values of mass and compliance can change (one going up while the other goes down proportionally) while maintaining the same resonance frequency, but the $M_A/C_A$ ratio changes and, therefore, $Q$ changes. Changing this ratio causes the resonance peak in the impedance magnitude to sharpen or broaden. A high $Q$ leads to a sharp resonance peak, where a low $Q$ leads to a broad resonance peak. It is important to note that although one is sharp and one is broad, if the resonance frequency and the resistance are kept constant, the values of the impedance minima will be the same (see Fig. 5). The pressure amplitude of the response of an individual resonator will also remain the same for a forced excitation.

The acoustic mass and compliance are constrained by physical necessity. One constraint that we used was to ensure that the acoustic mass and compliance must maintain the lumped-element characteristics of a Helmholtz resonator (though a higher order model for the resonator could have been used that would have modeled something like a quarter
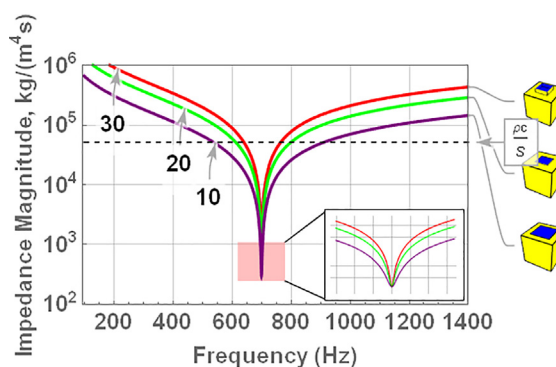


FIG. 5. (Color online) Impedance curves for three different shaped resonators. The quality factors of the resonators (going from top to bottom) are 30, 20, and 10. The acoustic impedance of a 4-in. diameter duct is also plotted as the dashed line. Resonance is 700 Hz. To increase visibility, the resonators shown are not scaled with size. Inset, impedance curves at resonance.

wavelength resonance and higher order modes along the resonator's length). This constraint means that every dimension of the neck and volume must be small compared to a wavelength so that no standing waves can form. To separate these regions and use the classical equations for resonance, it has been found[44] that the cross section of the neck must be less than ∼40% of the cross section of the volume.

A range of $Q$ was calculated with the physical constraints that the neck must be strictly less than $\lambda/4$ and the cavity must have the largest dimension less than $\lambda/4$. The minimum neck length is also restricted as its physical length goes to zero and only the acoustic end corrections remain, and this provides a nonzero lower bound to the acoustic mass. As the neck gets longer, the acoustic mass increases, but so does the thermoviscous resistance. For the examples given, the $Q$ was limited to a range of 10–30 (these values were determined for an individual resonator unattached to the waveguide). These resonators produce shapes like those found on the right side of Fig. 5.

Figure 5 shows that with the same resonance frequency, a lower $Q$ results in a broader impedance curve near their minima. A resonator couples well to the acoustic waves if it has an impedance similar to that of the waveguide. A broader impedance curve results in more frequencies close to the impedance of the waveguide and stronger interactions with the resonators. Thus, a lower $Q$ resonator will interact with the waves in the waveguide over a broader range of frequencies. It is similarly desirable to have a lower $Q$ when using Helmholtz resonators for filtering acoustic waves.[38] A lower $Q$ implies a smaller length neck, a large neck cross-sectional area, and a larger volume for the resonator.

Across the range of $Q$, competing priorities arise. Figure 6 shows that frequencies closer to the resonators' resonance frequency and resonators with a lower $Q$ lead to a smaller effective wavelength. However, in Fig. 7, it is apparent that the amplitude of the focus is lower in these conditions. Although a broader resonance peak allows the resonator to influence a greater range of frequencies and thus provide a sharper focus (as shown by the effective
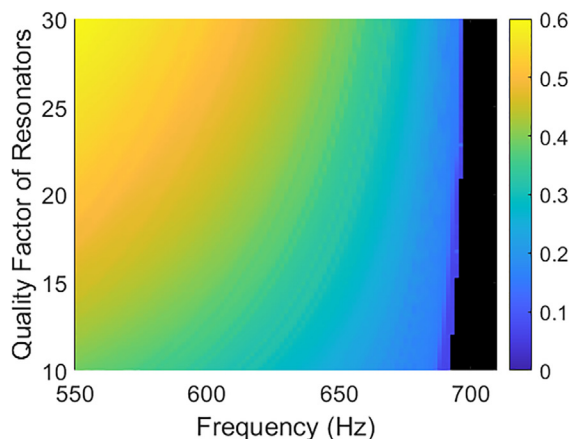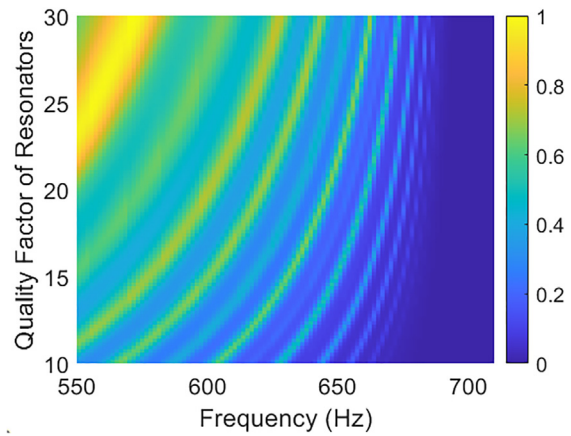


FIG. 7. (Color online) Amplitude of the focus across a range of quality factors and frequencies. The oscillations visible in the data are a result the maximum moving between resonators.

wavelength; Fig. 6), the amplitude of the focus also goes down (as shown by the focal amplitude; Fig. 7). These same competing priorities are found at every $Q$ as the frequency approaches resonance; the overall peak amplitude goes down, but the spatial extent of the focusing also becomes narrower. Thus, there is a trade-off between the spatial resolution one may obtain and the amplitude of the focusing. It was also found, when using a finite bandwidth of frequencies, that the sidelobe amplitudes become more comparable to the focal amplitude as the frequencies in the bandwidth approach the resonators' resonance frequency.

The oscillations visible in the amplitude dependence displayed in Fig. 7 are a result of attempting to focus between two resonators. Each of the sources produces a maximum near the focal location, but the maximum is always over a nearby resonator. As the source frequency changes, the maximum may move between resonators. The ability for the two sources to be in phase at the focal location is not always guaranteed.

As mentioned in the Introduction, part of the advantage of using equivalent circuits is the ability to explore the discretization of the space. Maznev *et al.* previously found that for single frequency focusing, the peak amplitude was always over a resonator, whether the intended focus location was over a resonator or not.[15] The equivalent circuit model treats the intersection of the resonator and the duct as occurring at a single point in space. Although this intersection is not physical, this behavior of the focusing reported in the experimental findings by Maznev *et al.* is replicated in the equivalent circuit model. Figure 8 shows the peak amplitude at the intended target location of the focusing as the target focal location is moved across the locations of four of the resonators, including attempts to focus sound at many locations between the resonators. Also shown is the spatial extent of two representative foci at 1.48 m (nearly exactly between resonators) and 1.517 m (near, but not exactly at, a resonator). Focusing near a resonator produces a higher amplitude. In fact, focusing near a resonator can produce a higher amplitude focus at other points than an attempt to



FIG. 6. (Color online) Fractional effective wavelength ($\lambda_{eff}/\lambda$) of waves among the resonators across a range of frequencies. Data omitted for undetermined effective wavelengths.

J. Acoust. Soc. Am. **152** (3), September 2022

Kingsley *et al.*    1269
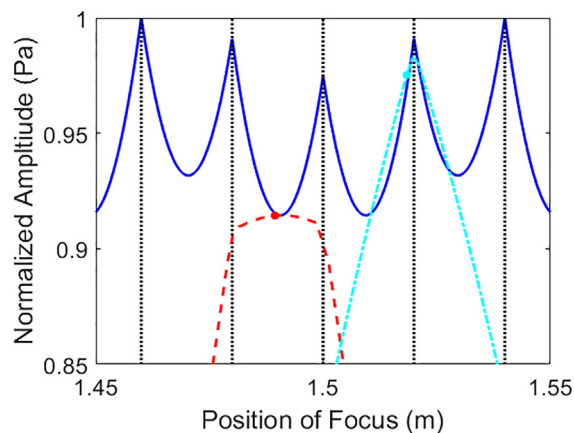
FIG. 8. (Color online) Amplitude of different foci as the target position is moved through a small range of positions near the middle of the set of resonators. The bandwidth is the same as in Fig. 3. Solid blue line, total amplitude at the focus location when TR is performed to focus a wave at that position. Dotted black lines, resonator positions. Red dashed line and cyan dotted-dashed line, spatial extent of the focus when focusing at 1.49 and 1.517 m, respectively. The focus location is marked with a dot.

focus at that point. This is shown in Fig. 8, where the (dotted-dashed cyan) focus occurring near the 1.52 m resonator produces amplitudes over an interval of 6.6 mm that are greater than an attempted focus at those positions. The resonators then are the target of the focusing, and reducing the spacing increases the focusing resolution. Thus, as stated by Maznev et al., no matter how small the FWHM may become, the space has been effectively discretized by the resonators, and the true resolution is that of the resonator spacing. It seems likely then that focusing between the resonators is simply a superposition of focusing at the adjacent resonators.

## V. CONCLUSION

An equivalent circuit model has been presented that describes the behavior of waves in a phononic crystal with finite length and anechoic terminations. The model has been verified by comparing the phase speed to results from the literature. Effects among the resonators that have been previously observed in experiments have been observed in the equivalent circuit model. It has been shown that the presence of the resonators decreases the phase speed and leads to super-resolution when combined with TR focusing techniques. The quality factor of the resonators has been explored, and it has been shown that broadband focusing is more easily achieved with low quality factors when the resistance is kept constant. The trade-off between resolution and focal amplitude, and hence the quality of the focusing (here lower quality focusing means high sidelobe amplitudes relative to the focal amplitude), has also been explored, with frequencies near resonance yielding better spatial resolution but also contributing lower amplitude toward the focusing over a bandwidth of frequencies. This model can be used to explore other phononic crystal configurations in one dimension to obtain both phase speed behaviors and wave-resonator interactions.

This equivalent circuit model fits the analytical models as presented by Sugimoto et al. when looking at the effect of the medium on the large-scale parameter of phase speed. Although the methods of arriving at the phase speed are very different, the close agreement in the results shows that the equivalent circuit model can describe a crystal as if it were an effective medium. It also can be used to study waves within the crystal, and results match the small-scale effect of the focus snapping to an individual resonator as seen in the experimental results of Maznev et al. Although super-resolution has been shown, it has also been shown that the limiting resolution is the placement of the resonators, which serve as the effective measurement apparatus, with the resonators acting as individual pixels, and a focusing resolution below the spacing of the resonators is not possible.

The equivalent circuit model can describe large and small effects that are exhibited by a wave traversing a 1-D phononic crystal. This model has been used to parameterize some of the physical variables present in the model and has shown that the $Q$ influences the bandwidth of contributing frequencies. This model has been shown to be useful for exploring this model and can describe other configurations. Previous work in phononic crystals has explored the influence of losses and alternating resonance frequencies on the absorption and phase speed of the waves.[25] This model could be used to explore additional and arbitrary complications in the configuration of resonators.

## ACKNOWLEDGMENTS

[1]M. Fink, "Time reversed acoustics," Phys. Today 50(3), 34–40 (1997).

[2]B. E. Anderson, M. Griffa, C. Larmat, T. J. Ulrich, and P. A. Johnson, "Time reversal," Acoust. Today 4(1), 5–16 (2008).

[3]B. E. Anderson, M. C. Remillieux, P.-Y. L. Bas, and T. J. Ulrich, "Time reversal techniques," in Nonlinear Acoustic Techniques for Nondestructive Evaluation, 1st ed., edited by T. Kundu (Acoustical Society of America, New York), pp. 547-581 (2018).

[4]A. Parvulescu and C. S. Clay, "Reproducibility of signal transmissions in the ocean," Radio Electron. Eng. 29(4), 223–228 (1965).

[5]C. S. Clay and B. E. Anderson, "Matched signals: The beginnings of time reversal," Proc. Meet. Acoust. 12(1), 055001 (2011).

[6]C. S. Larmat, R. A. Guyer, and P. A. Johnson, "Time-reversal methods in geophysics," Phys. Today 63(8), 31–35 (2010).

[7]G. Montaldo, P. Roux, A. Derode, C. Negreira, and M. Fink, "Ultrasound shock wave generator with one-bit time reversal in a dispersive medium, application to lithotripsy," Appl. Phys. Lett. 80, 897–899 (2002).

[8]R. K. Ing and N. Quieffin, "In solid localization of finger impacts using acoustic time-reversal process," Appl. Phys. Lett. 87(20), 204104 (2005).

[9]S. Cheinet, L. Ehrhardt, and T. Broglin, "Impulse source localization in an urban environment: Time reversal versus time matching," J. Acoust. Soc. Am. 139(1), 128–140 (2016).

[10]C. Larmat, J.-P. Montagner, M. Fink, Y. Capdeville, A. Tourin, and E. Clévédé, "Time-reversal imaging of seismic sources and application to the great Sumatra earthquake," Geophys. Res. Lett. 33, L19312, https://doi.org/10.1029/2006GL026336 (2006).

[11]B. E. Anderson, M. Griffa, T. J. Ulrich, and P. A. Johnson, "Time reversal reconstruction of finite sized sources in elastic media," J. Acoust. Soc. Am. **130**(4), EL219–EL225 (2011).

[12]A. A. Maznev and O. B. Wright, "Upholding the diffraction limit in the focusing of light and sound," Wave Motion **68**, 182–189 (2017).

[13]G. Lerosey, J. de Rosny, A. Tourin, and M. Fink, "Focusing beyond the diffraction limit with far-field time reversal," Science **315**(5815), 1120–1122 (2007).

[14]F. Lemoult, M. Fink, and G. Lerosey, "Acoustic resonators for far-field control of sound on a subwavelength scale," Phys. Rev. Lett. **107**(6), 064301 (2011).

[15]A. A. Maznev, G. Gu, S. Y. Sun, J. Xu, Y. Shen, N. Fang, and S. Y. Zhang, "Extraordinary focusing of sound above a soda can array without time reversal," New J. Phys. **17**, 042001 (2015).

[16]G. Ma, X. Fan, F. Ma, J. de Rosny, P. Sheng, and M. Fink, "Towards anti-causal Green's function for three-dimensional sub-diffraction focusing," Nat. Phys. **14**(6), 608–612 (2018).

[17]A. Mimani, "A point-like enhanced resolution of experimental Aeolian tone using an iterative point-time-reversal-sponge-layer damping technique," Mech. Syst. Signal Process. **151**, 107411 (2021).

[18]S. G. Conti, P. Roux, and W. A. Kuperman, "Near-field time-reversal amplification," J. Acoust. Soc. Am. **121**(6), 3602–3606 (2007).

[19]J. de Rosny and M. Fink, "Overcoming the diffraction limit in wave physics using a time-reversal mirror and a novel acoustic sink," Phys. Rev. Lett. **89**(12), 124301 (2002).

[20]F. Ma, J. Chen, J. Wu, and H. Jia, "Realizing broadband sub-wavelength focusing and a high intensity enhancement with a space-time synergetic modulated acoustic prism," J. Mater. Chem. C **8**, 9511–9519 (2020).

[21]F. Ma, Z. Huang, C. Liu, and J. H. Wu, "Acoustic focusing and imaging via phononic crystal and acoustic metamaterials," J. Appl. Phys. **131**, 011103 (2022).

[22]M.-H. Lu, L. Feng, and Y.-F. Chen, "Phononic crystals and acoustic metamaterials," Mat. Today **12**(12), 34–42 (2009).

[23]X. Wang and C. M. Mak, "Acoustic performance of a duct loaded with identical resonators," J. Acoust. Soc. Am. **131**(4), EL316–EL322 (2012).

[24]Z. G. Wang, S. H. Lee, C. K. Kim, C. M. Park, K. Nahm, and S. A. Nikitov, "Acoustic wave propagation in one-dimensional phononic crystals containing Helmholtz resonators," J. Appl. Phys. **103**(6), 064907 (2008).

[25]J. Guo, J. Cao, Y. Xiao, H. Shen, and J. Wen, "Interplay of local resonances and Bragg band gaps in acoustic waveguides with periodic detuned resonators," Phys. Lett. A **384**(13), 126253 (2020).

[26]C. E. Bradley, "Acoustic Bloch wave propagation in a periodic waveguide," Technical report of Applied Research Laboratories, ARL-TR- 91-19 (July), University of Texas, Austin, TX, 1991.

[27]N. Sugimoto and T. Horioka, "Dispersion characteristics of sound waves in a tunnel with an array of Helmholtz resonators," J. Acoust. Soc. Am. **97**(3), 1446–1459 (1995).

[28]M. Tanter, J. Thomas, and M. Fink, "Time reversal and the inverse filter," J. Acoust. Soc. Am. **108**(1), 223–234 (2000).

[29]B. E. Anderson, R. A. Guyer, T. J. Ulrich, and P. A. Johnson, "Time reversal of continuous-wave, steady-state signals in elastic media," Appl. Phys. Lett. **94**(11), 111908 (2009).

[30]G. Bertuccio, "On the physical origin of the electro-mechano-acoustical analogy," J. Acoust. Soc. Am. **151**(3), 2066–2076 (2022).

[31]B. B. Bauer, "Equivalent circuit analysis of mechano-acoustic structures," Trans. IRE Prof. Group Audio **AU-2**(4), 112–120 (1954).

[32]B. E. Anderson, C. B. Hilton, and F. Giorgini, "Equivalent circuit modeling and vibrometry measurements of the Nigerian-origin Udu Utar drum," J. Acoust. Soc. Am. **133**(3), 1718–1726 (2013).

[33]C. B. Goates, M. F. Calton, S. D. Sommerfeldt, and D. C. Copley, "Modeling acoustic resonators using higher-order equivalent circuits," Noise Control Eng. J. **67**(6), 456–466 (2019).

[34]S. Pyo and Y. Roh, "Structural design of an acoustic planar array transducer by using the equivalent circuit method," Ultrasonics **108**, 106219 (2020).

[35]B. E. Anderson and S. D. Sommerfeldt, "Solving one-dimensional acoustic systems using the impedance translation theorem and equivalent circuits: A graduate level homework assignment," J. Acoust. Soc. Am. **150**(6), 4155–4165 (2021).

[36]E. Brandão, W. D. Fonseca, and P. H. Mareze, "An algorithmic approach to electroacoustical analogies," J. Acoust. Soc. Am. **152**(1), 667–678 (2022).

[37]W. P. Mason, *Electromechanical Transducers and Wave Filters* (Van Nostrand, New York, 1942), pp. 204–205.

[38]U. Ingard, "On the theory and design of acoustic resonators," J. Acoust. Soc. Am. **25**(6), 1037–1061 (1953).

[39]L. E. Kinsler, A. R. Frey, A. B. Coppens, and J. V. Sanders, *Fundamentals of Acoustics*, 4th ed. (Wiley, New York, 2000), pp. 284–286.

[40]H. von Helmholtz, "Ueber einige Gesetze der Vertheilung elektrischer Ströme in körperlichen Leitern mit Anwendung auf die thierisch-elektrischen Versuche" ("Some laws concerning distribution electrical currents conductors with applications to experiments animal electricity"), Ann. Phys. Chem. **165**(6), 211–233 (1853).

[41]M. H. Denison and B. E. Anderson, "Time reversal acoustics applied to rooms of various reverberation times," J. Acoust. Soc. Am. **144**(6), 3055–3066 (2018).

[42]J. V. Candy, A. J. Poggio, D. H. Chambers, B. L. Guidry, C. L. Robbins, and C. A. Kent, "Multichannel time-reversal processing for acoustic communications in a highly reverberant environment," J. Acoust. Soc. Am. **118**, 2339–2354 (2005).

[43]S. Yon, M. Tanter, and M. Fink, "Sound focusing in rooms: The time-reversal approach," J. Acoust. Soc. Am. **113**(3), 1533–1543 (2003).

[44]R. L. Panton and J. M. Miller, "Resonant frequencies of cylindrical Helmholtz resonators," J. Acoust. Soc. Am. **57**(6), 1533–1535 (1975).

J. Acoust. Soc. Am. **152** (3), September 2022

Kingsley *et al.*    1271